4-2013

MeV-Energy X Rays from Inverse Compton Scattering with Laser-Wakefield Accelerated Electrons

Donald Umstadter
University of Nebraska-Lincoln, donald.umstadter@unl.edu

Shouyuan Chen
University of Nebraska-Lincoln, schen6@unl.edu

Nathan D. Powers
University of Nebraska-Lincoln, ndp5@byu.edu

I. Ghebregziabher
University of Nebraska - Lincoln

C. Maharjan
University of Nebraska - Lincoln

See next page for additional authors

MeV-Energy X Rays from Inverse Compton Scattering with Laser-Wakefield Accelerated Electrons

S. Chen,[1] N. D. Powers,[1] I. Ghebregziabher,[1] C. M. Maharjan,[1] C. Liu,[1] G. Golovin,[1] S. Banerjee,[1] J. Zhang,[1] N. Cunningham,[1,*] A. Moorti,[1,†] S. Clarke,[2] S. Pozzi,[2] and D. P. Umstadter[1,‡]

[1]*Department of Physics and Astronomy, University of Nebraska, Lincoln, Nebraska 68588, USA*

[2]*Department of Nuclear Engineering and Radiological Sciences, University of Michigan, Ann Arbor, Michigan 48109, USA*

(Received 21 November 2012; published 10 April 2013)

We report the generation of MeV x rays using an undulator and accelerator that are both driven by the same 100-terawatt laser system. The laser pulse driving the accelerator and the scattering laser pulse are independently optimized to generate a high energy electron beam (> 200 MeV) and maximize the output x-ray brightness. The total x-ray photon number was measured to be $\sim 1 \times 10^7$, the source size was 5 μm, and the beam divergence angle was ~ 10 mrad. The x-ray photon energy, peaked at 1 MeV (reaching up to 4 MeV), exceeds the thresholds of fundamental nuclear processes (e.g., pair production and photodisintegration).

DOI: 10.1103/PhysRevLett.110.155003 PACS numbers: 52.38.Ph, 41.60.Ap, 52.38.Kd

By generating x rays with photon energy reaching the MeV level, inverse-Compton-scattering sources (also referred to as Thomson sources) have enabled the use of synchrotron light for nuclear physics research, as well as for numerous novel radiological applications [1–3]. Compton sources are usually quite large (> 100 m) because they rely on large conventional electron accelerators. They can, however, be substantially smaller—and yet generate bright x rays—when driven instead by a compact advanced laser-wakefield electron accelerator (LWFA), which can accelerate electrons to GeV energy in a distance of only a few centimeters [4–6].

In a previous study of a LWFA-based Compton source, only soft x rays (~ 1 keV) without beam properties are reported [7]. More recently, a single laser pulse is used to both accelerate the electrons and scatter (after reflection from a plasma mirror) [8]. While hard x rays are produced in this latter case (peaked at ~ 50 keV), the photon energy is still well below the thresholds for photonuclear processes.

We report here an all-optical-driven Compton scattering source of γ ray energy x rays. The x-ray output parameters could be optimized by employing two independent laser pulses from the same high-peak-power laser system—one pulse optimized for accelerating electrons by a laser wakefield, and the other pulse optimized for Compton scattering. The electron beam and scattering pulse were spatially overlapped (and temporally synchronized) with micron (femtosecond) accuracy. Besides optimization of the x-ray output, the ability to independently adjust the parameters of the two laser pulses has several other advantages. It permits scalability to higher γ-ray flux with increasing scattering laser pulse energy. A cross-correlation technique was used to characterize the source sizes of both the electron beam and γ-ray beam, by scanning the scattering laser pulse across the electron beam. This design is also free from the debris contamination and bremsstrahlung background, both of which are inherent to the single-laser-pulse approach [8]. Characterization of higher energy x rays required both the development of a novel detection method as well as implementation of a novel numerical scattering model.

The experiments were conducted using the 100-TW Diocles laser at the University of Nebraska, Lincoln, which operates with a 10-Hz repetition rate, and at a central wavelength of 800 nm [9]. The accelerator drive pulse and scattering pulse were both generated from the same laser pulse by means of an optical beam splitter with 80/20 percent split ratio. A deformable mirror corrected the wave front and improved the focal quality of both beams. Figure 1 shows the schematic of the setup. The 1.9-J, 35-fs drive laser pulse was focused by a 1-m focal length parabolic reflector onto a 2-mm supersonic gas target (mixture of 99% helium and 1% nitrogen) with a Gaussian full width at half maximum (FWHM) focal spot size of 20 μm. 33% of the laser energy of the driven pulse was enclosed in the FWHM width, and it corresponded to a peak intensity of 7.4×10^{18} W/cm^2 (normalized vector potential of $a_0 = 1.9$). The plasma density of the target was 1.0×10^{19}/cm^3. As such, the LWFA was operated in the ionization-injected, self-guided, and bubble regime [10,11]. The energy and the charge of generated electron beam (e beam) were monitored by a magnetic spectrometer, consisting of a calibrated LANEX screen and imaged by a 12-bit CCD camera, on every shot. The magnetic spectrometer has an energy cutoff around 50 MeV due to the size of the LANEX screen. The electron beam is optimized in the experiment, in terms of energy and charge, by controlling both the plasma density and the focal position of the driving laser beam (relative to the gas target). With these optimizations, electron beams were produced with cutoff energy ~ 250 MeV, and total integrated charge of ~ 0.1 nC (for energies > 50 MeV). The 0.5-J, 90-fs scattering laser beam was focused by a 1-m focal length lens. To take into account the effect of the B

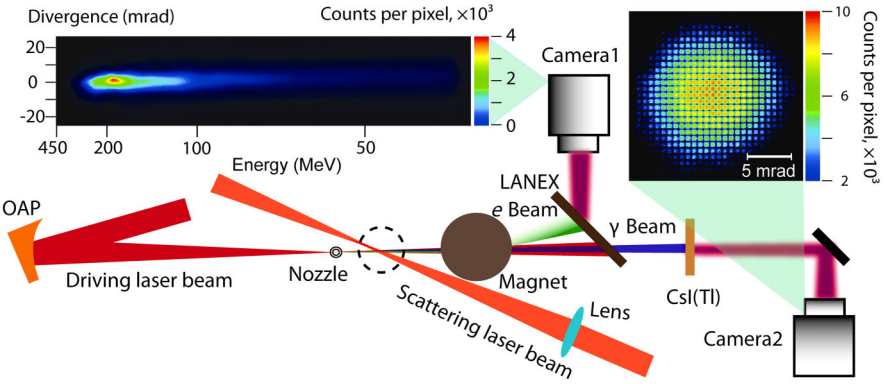

FIG. 1 (color online). All-laser-driven Compton γ-ray source. Schematic of the experimental setup. Left inset shows the electron energy spectrum as recorded by the LANEX screen, which was imaged by CCD camera. Right inset shows the γ-ray beam profile measured by pixelated CsI(Tl) scintillator imaged by EMCCD camera.

integral of the focusing lens and beam splitter on the focus spot quality at high laser power, the scattering laser beam focal spot was measured with the same laser power used in the experiment. The measured focal spot was 22 μm FWHM (rms spot size $\sigma_L = 9$ μm) with 16% of its energy enclosed in the FWHM width as shown in Fig. 2, corresponding to a peak focused intensity of 3.4×10^{17} W/cm^2 ($a_0 = 0.4$). Figure 2 shows the overlapping geometry, in which the scattering laser beam counter-propagates at an angle of $\Phi = 170°$ (in the horizontal plane) to the e beam. The interaction point was located in the vacuum region 1 mm downstream from the exit of the laser plasma accelerator [12].

From the energy scaling formula of Compton scattering $E_\gamma = 4\gamma^2 E_L$, where E_γ is the γ-ray photon energy, γ is the electron relativistic factor and E_L is the laser photon energy, we expect to generate a 1.4 MeV γ ray by scattering 1.5 eV photons off 250 MeV electron beam. To detect and characterize the high energy x-ray beam generated in this experiment with optimal response and high spatial resolution, we used a CsI-crystal scintillator, which consisted of a 1-cm deep, 40×40 array of $1.0 \times 1.0 \times 10$-mm "voxels" (3D pixels), with a 0.2-mm epoxy layer between voxels (Dynasil Corporation, Massachusetts, USA).

The CsI(Tl) scintillator was placed on axis ($\Phi = 180°$) at a distance of 1.72 m from the interaction point. The optical light signal from the CsI(Tl) detector was imaged onto a 14-bit EMCCD camera. This γ-ray detection system

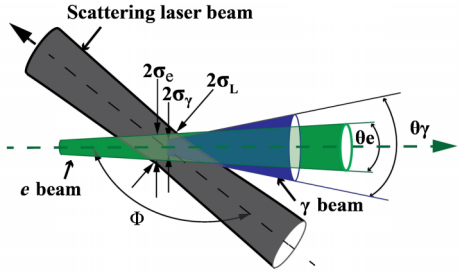

FIG. 2 (color online). Interaction geometry defining beam parameters.

was calibrated using a Cs^{137} radiation source of known activity. A lead baffle was placed in front of the scintillator to shield the detector from background noise, and the detection system had a signal to noise ratio of 20:1. Figure 1 (right inset) shows a typical background-subtracted single-shot image of the γ-ray beam with the corresponding e-beam spectrum shown in Fig. 1 (left inset). The γ-ray beam typically had a ~10-mrad divergence angle, a near-circular shape, and a Gaussian profile. With a consecutive run of 50 laser shots, γ-ray beams were observed in 90% percent of these shots. The fluctuation was mainly due to the electron beam pointing fluctuation, which can be determined from the electron beam angular position on the LANEX screen. No γ rays were observed in any of the ~400 laser shots for which the scattering beam was blocked.

Several theoretical predictions have been made for the performance of Compton sources when LWFA e beams are used [13]. We developed our own benchmarked numerical code to calculate the angle-resolved γ-ray spectrum [14], using the experimentally measured characteristics of the scattering laser beam and e beam (see Table I) as input. The simulated γ-ray parameters were then used as the input for a Monte Carlo simulation (MCNPX code) in order to produce a simulated γ-ray beam profile image [15], which could be compared to the measured one, shown in Fig. 1 (right inset). With the input electron beam six dimension phase space parameters reconstructed from the energy spectrum and divergence angle shown in Fig. 1 (left inset), the simulated γ-ray beam profile had a divergence of 11.3 mrad, which had a good agreement with the experimentally measured value, 12.7 mrad. The simulation also predicted a total photon number of 2×10^7, which had reasonable agreement with the experimentally measured photon number of $\sim 1 \times 10^7$.

To reveal the γ-ray spectrum, a quadrant filter (crossed plates of 1.7 mm lead and 3.4 mm lead) is placed in front of the CsI detector. The measured quad-filtered image is shown in Fig. 3(c). The transmittance of different thickness filters at different divergence angles is shown in Fig. 3(d).

TABLE I. Typical experimental parameters for scattering laser (ω_0), electron (e), and gamma (γ) beams.

Beam	Parameter	Symbol	Value
ω_0	Energy	E_{laser}	0.5 J/pulse
	Wavelength	λ	800 nm
	Pulse duration	τ_s	90 fs (FWHM)
	Spot size	σ_L	9 ± 1 μm (rms)
	Number of laser oscillations/pulse	N_{laser}	34
	Average power	P_L	5.6 TW
	Normalized field strength	a_0	0.4
	Photon energy	E_L	1.5 eV
	Interaction angle	Φ	170 deg
e	Source size	σ_e	6 ± 3 μm (rms)
	Cutoff energy[a]	E_c	250 MeV
	Divergence[b]	θ_e	5 mrad (FWHM)
	Total charge	Q	120 pC
γ	Source size	σ_γ	5 ± 3 μm (rms)
	Divergence	θ_γ	12.7 mrad (FWHM)
	Peak energy	E_γ	1.2 MeV
	Photons/pulse	N_γ	$\sim 10^7$
	Peak on axis brilliance	B_x	$\sim 1 \times 10^{19}$ photons s^{-1}-mm^{-2}-mrad^{-2} (per 0.1% BW)

[a]Corresponds to energy at 10% of the peak value of the electron spectrum.
[b]Corresponds to the divergence of the beam at the cutoff energy.

The transmittance measurement not only showed the x-ray source has high photon energy because of the penetration of 5.1 mm lead, but also revealed angular dependence of the x-ray source spectrum, since transmittance is lower at large divergence angle for each quadrant.

Based on the measured e-beam energy spectrum, shown in Fig. 3(a) (inset), a simulated on axis γ-ray intensity spectrum is obtained, as shown in Fig. 3(a), which is peaked at 1 MeV and extends to 4 MeV. Simulated x-ray spectra for each angle were used to create a simulated image of filtered γ-ray beam profile. Comparisons of the simulated and measured x-ray transmission levels through the various filter thicknesses and at various polar angles are shown in Fig. 3(d). [The error bars in Fig. 3(d) originate from uncertainties in the background subtraction levels, and the beam-center location on the CsI.] The analysis shows that the simulated and measured transmittances agree within the experimental uncertainty, and thus the simulated spectrum can be used to represent the experimental spectrum. To show the peak-energy sensitivity of our quad filter-based measurement, we shifted the simulated x-ray spectrum with 0.1 MeV steps from -0.6 to $+0.6$ MeV, and reconstructed CsI images for each step (See Supplemental Material [16] for sensitivity of quadrant filter measurement relative to

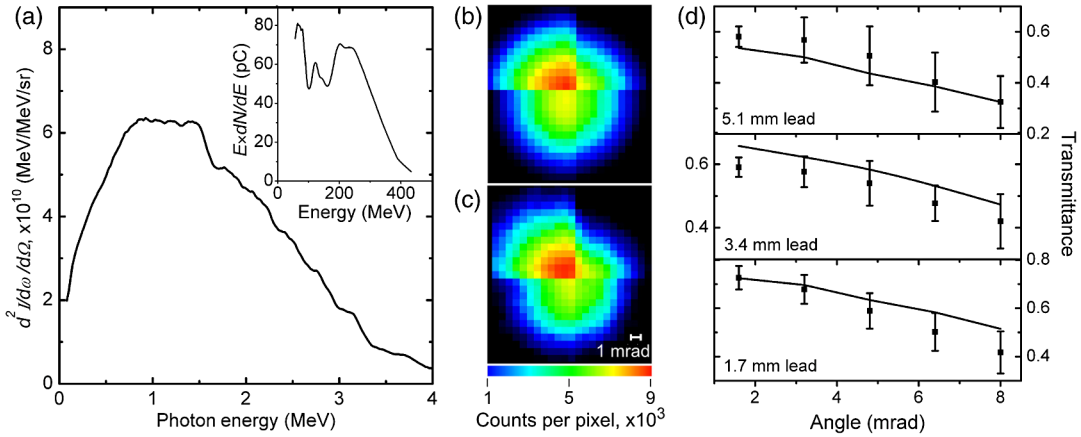

FIG. 3 (color online). γ-ray spectrum. (a) Simulated on axis γ-ray spectrum, with corresponding e-beam spectrum (inset). (b) Simulated γ-ray beam profile transmitted through quad filter (not attenuated at top-left corner, 1.7 mm lead at top-right, 3.4 mm lead at bottom-left, 5.1 mm lead at bottom-right). (c) Measured γ-ray beam profile transmitted through quad filter. (d) Comparison between simulated and measured γ-ray transmittances through different filters, as a function of divergence angle. The solid line represents the simulated transmittance and squares represent the measured transmittance.

spectra peak shift). To estimate the similarity between these images and an experimentally measured one, we took the difference of the images (normalized-measured minus normalized-simulated) and calculated the mean and standard deviation (SD) for each image. Both figures of merits are close to their minima for unshifted spectrum, demonstrating that the quadrant filters method has a peak sensitivity of at least ± 0.2 MeV.

Another important parameter of the γ-ray source is the source size. Methods based on diffraction, which are usually used to measure the source size of keV x rays [8,17,18], cannot be applied to the γ-ray source due to the high photon energy ($\sim$ MeV). Instead, we exploit the spatial cross-correlation technique to measure the radiation source size [19–22], in which the scattering beam focal spot was scanned vertically across the e beam over a spatial range of 90 μm. The shots with similar electron beam pointing and spectra were first selected from each scanning position. The recorded γ-ray beam profiles were then analyzed, and the resulting photon yield, as a function of radius, is shown in Fig. 4. A Gaussian spatial profile is assumed for both the laser and e beam, with the width of the cross-correlation profile given by $\sigma_{\text{signal}} = (\sigma_L^2 + \sigma_e^2)^{1/2}$, where σ_e and σ_L are the rms widths of electron beam and laser beam, respectively, at the interaction point. A Gaussian profile was fitted to the data points and the best fit was obtained with $\sigma_{\text{signal}} = 11$ μm with a fitting error of ± 1 μm. With the measured focal spot size of the laser pulse, $\sigma_L = 9$ with a measurement error of ± 1 μm, and width of the cross-correlation trace, the e-beam size was estimated, by deconvolution of the cross-correlation curve, to be $\sigma_e = 6 \pm 3$ μm. The γ-ray source size σ_γ is given

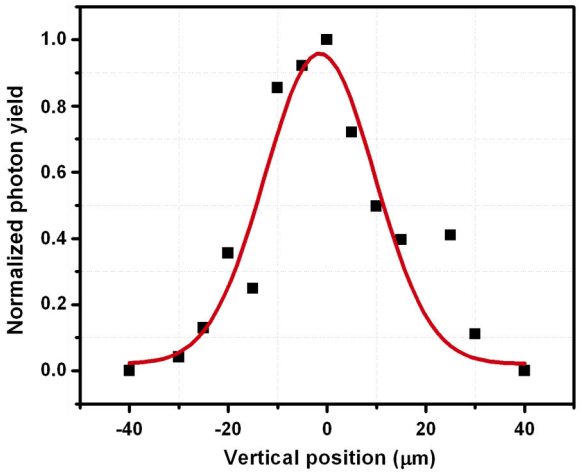

FIG. 4 (color online). γ-ray and electron radiation source size measurements. Normalized γ-ray yield as a function of the laser pulse vertical position. Each data point represents the γ-ray yield obtained by integrating over a single-shot background-subtracted γ-ray beam profile image. The solid line is a Gaussian fit with an rms width of 11 ± 1 μm. By deconvolving the cross-correlation trace, we estimate the rms width of the e-beam size at the interaction point to be 6 ± 3 μm.

by the products of electron and laser beam distribution $\sigma_\gamma = \sigma_L \sigma_e / (\sigma_L^2 + \sigma_e^2)^{1/2}$, and $\sigma_\gamma = 5 \pm 3$ μm. The error in the source-size measurement is mainly attributed to uncertainty of the electron and laser beam positions relative to each other ($\sigma_{\text{uncertainty}} = \pm 4$ μm).

The peak on axis x-ray brightness is estimated to be of the order of 1×10^{19} photons $\text{s}^{-1}\,\text{mm}^{-2}\,\text{mrad}^{-2}$ (per 0.1% BW) at photon energies ranging from 0.9 to 1.4 MeV. This estimate is based on our γ-ray results, reported above, and e-beam pulse duration of 35 fs (from previous relevant LWFA measurements [23,24]). The energy conversion efficiency from scattering laser pulse to γ-ray beam is in the order of $\sim 10^{-6}$.

The e-beam and scattering beam parameters are nearly optimal for Compton efficiency. The scattering beam was focused to as high an intensity as possible ($a = 0.4$) to maximize the undulator strength, but not too high to generate nonlinear effects [25,26]. Its focal spot size (9 μm) was also chosen to closely match the size of the e beam (6 μm) at the interaction point. This helps to increase the Compton scattering efficiency as the yield of Compton photon is inversely proportional to overlapping area. Additionally, both pulses—by virtue of being driven by the same laser system—were synchronized in time to each other, which eliminated timing jitter and allowed ultrashort duration pulses to be used without large fluctuations in their temporal overlap, and consequently the γ-ray output.

Besides providing a measurement of our γ-ray radiation source size, our Compton cross-correlation method also provided information on the LWFA e beam. The source size of the e beam [2 μm (rms)] was extrapolated from both the e-beam size measured at the Compton interaction point [6 μm (rms)] and its average divergence angle (10 mrad), assuming the space-charge blowup is negligible for our e-beam charge density and average energy [27]. Using the inferred source size, and the measured divergence angle of 5 mrad (for the 250-MeVcomponent of the e beam), we estimate a normalized rms e-beam emittance ($\varepsilon_N = \sigma_{e\text{-source}} \gamma \theta_{250\,\text{MeV}}$) of 1 mm-mrad at 250 MeV. This technique provides another method to characterize the emittance of an LWFA electron beam, adding to the pepperpot and betatron radiation techniques that have already been reported [28–31].

In conclusion, γ rays generated by all-optical-driven electron acceleration and Compton scattering were found to have total photon number of 2×10^7, divergence of ~ 10 mrad, radiation source size of 5 μm, and peak brightness of 10^{19} photons $\text{s}^{-1}\,\text{mm}^{-2}\,\text{mrad}^{-2}$ (per 0.1% BW). The γ ray generation combined with a cross-correlation technique helped to characterize the properties of the electron beam generated from the LWFA. The current source has an on axis *intensity* spectrum that peaks at photon energy of 1 MeV, even though the *photon-number* spectrum (without weighting by the photon energy) does not appear peaked. In future experiments, even the photon-number x-ray spectrum would be peaked if the more monoenergetic

electron beams that have recently been demonstrated [32–35] were to be used. Wide tunability range and micron radiation source size would also be achieved, which could help to improve radiography and radiotherapy [36–38]. For example, with the current setup, a 200-MeV electron beam with a 6% energy spread (FWHM) will generate a 0.8-MeV energy γ-ray beam with 24% energy spread (FWHM), when integrated over a $1/\gamma$ radiation cone angle. MeV photon energy, combined with ultrashort pulse duration (fs), may also enable exploration of a new research direction; namely, ultrafast nuclear science [39,40].

We thank V. Ramanathan, N. Chandler-Smith, K. Brown, and J. Mills for their contributions to the laser facility. This material is based upon work supported by the U.S. Department of Energy (Grant No. DE-FG02-05ER15663), Defense Threat Reduction Agency (Grant No. HDTRA1-11-C-0001), Air Force Office for Scientific Research (Grants No. FA 9550-08-1-0232, and No. FA9550-11-1-0157), Department of Homeland Security (Grant No. 2007-DN-077-ER0007-02), and Defense Advanced Research Projects Agency (Grant No. FA9550-09-1-0009).

*Present address: Physics Department, Nebraska Wesleyan University, Lincoln, Nebraska 68504, USA.

†Present address: Raja Ramanna Centre for Advanced Technology, Indore 452 013, India.

‡Author to whom correspondence should be addressed. donald.umstadter@unl.edu

[1] E. Kwan, G. Rusev, A. S. Adekola *et al.*, Phys. Rev. C **83**, 041601 (2011).
[2] E. C. Schreiber, R. S. Canon, B. T. Crowley *et al.*, Phys. Rev. C **61**, 061604 (2000).
[3] F. Albert, S. G. Anderson, G. A. Anderson *et al.*, Opt. Lett. **35**, 354 (2010).
[4] T. Tajima and J. M. Dawson, Phys. Rev. Lett. **43**, 267 (1979).
[5] D. Umstadter, S. Y. Chen, A. Maksimchuk, G. Mourou, and R. Wagner, Science **273**, 472 (1996).
[6] E. Esarey, C. B. Schroeder, and W. P. Leemans, Rev. Mod. Phys. **81**, 1229 (2009).
[7] H. Schwoerer, B. Liesfeld, H. P. Schlenvoigt, K. U. Amthor, and R. Sauerbrey, Phys. Rev. Lett. **96**, 014802 (2006).
[8] K. T. Phuoc, S. Corde, C. Thaury, V. Malka, A. Tafzi, J. P. Goddet, R. C. Shah, S. Sebban, and A. Rousse, Nat. Photonics **6**, 308 (2012).
[9] V. Ramanathan, S. Banerjee, N. Powers *et al.*, Phys. Rev. ST Accel. Beams **13**, 104701 (2010).
[10] A. Pak, K. A. Marsh, S. F. Martins, W. Lu, W. B. Mori, and C. Joshi, Phys. Rev. Lett. **104**, 025003 (2010).
[11] C. McGuffey, A. G. R. Thomas, W. Schumaker *et al.*, Phys. Rev. Lett. **104**, 025004 (2010).
[12] S. Banerjee, S. Sepke, R. Shah, A. Valenzuela, A. Maksimchuk, and D. Umstadter, Phys. Rev. Lett. **95**, 035004 (2005).
[13] F. V. Hartemann, D. J. Gibson, W. J. Brown, A. Rousse, K. T. Phuoc, V. Mallka, J. Faure, and A. Pukhov, Phys. Rev. ST Accel. Beams **10**, 011301 (2007).
[14] I. Ghebregziabher, B. Shadwick, and D. Umstadter, Phys. Rev. ST Accel. Beams **16**, 030705 (2013).
[15] D. B. Pelowitz, MCNPX Manual, Version 2.7.0., Report No. LA-CP-11-00438, 2011.
[16] See Supplemental Material at http://link.aps.org/supplemental/10.1103/PhysRevLett.110.155003 for sensitivity of quadrant filter measurement.
[17] R. C. Shah, F. Albert, K. Ta Phuoc, O. Shevchenko, D. Boschetto, A. Pukhov, S. Kiselev, F. Burgy, J.-P. Rousseau, and A. Rousse, Phys. Rev. E **74**, 045401 (2006).
[18] S. Kneip, C. McGuffey, J. L. Martins *et al.*, Nat. Phys. **6**, 980 (2010).
[19] R. Alley, D. Arnett, E. Bong *et al.*, Nucl. Instrum. Methods Phys. Res., Sect. A **379**, 363 (1996).
[20] H. Sakai, Y. Honda, N. Sasao, S. Araki, Y. Higashi, T. Okugi, T. Taniguchi, J. Urakawa, and M. Takano, Phys. Rev. ST Accel. Beams **4**, 022801 (2001).
[21] W. P. Leemans, R. W. Schoenlein, P. Volfbeyn, A. H. Chin, T. E. Glover, P. Balling, M. Zolotorev, K. J. Kim, S. Chattopadhyay, and C. V. Shank, Phys. Rev. Lett. **77**, 4182 (1996).
[22] S. T. Boogert, G. A. Blair, G. Boorman *et al.*, Phys. Rev. ST Accel. Beams **13**, 122801 (2010).
[23] A. D. Debus, M. Bussmann, U. Schramm *et al.*, Phys. Rev. Lett. **104**, 084802 (2010).
[24] J. van Tilborg, C. B. Schroeder, C. V. Filip, C. Toth, C. G. R. Geddes, G. Fubiani, R. Huber, R. A. Kaindl, E. Esarey, and W. P. Leemans, Phys. Rev. Lett. **96**, 014801 (2006).
[25] S. Y. Chen, A. Maksimchuk, and D. Umstadter, Nature (London) **396**, 653 (1998).
[26] Y. Y. Lau, F. He, D. P. Umstadter, and R. Kowalczyk, Phys. Plasmas **10**, 2155 (2003).
[27] G. Fubiani, J. Qiang, E. Esarey, W. P. Leemans, and G. Dugan, Phys. Rev. ST Accel. Beams **9**, 064402 (2006).
[28] S. Fritzler, E. Lefebvre, V. Malka, F. Burgy, A. E. Dangor, K. Krushelnick, S. P. D. Mangles, Z. Najmudin, J. P. Rousseau, and B. Walton, Phys. Rev. Lett. **92**, 165006 (2004).
[29] E. Brunetti, R. P. Shanks, G. G. Manahan *et al.*, Phys. Rev. Lett. **105**, 215007 (2010).
[30] S. Kneip, C. McGuffey, J. L. Martins *et al.*, Phys. Rev. ST Accel. Beams **15**, 021302 (2012).
[31] M. Schnell, A. Savert, B. Landgraf *et al.*, Phys. Rev. Lett. **108**, 075001 (2012).
[32] B. B. Pollock, C. E. Clayton, J. E. Ralph *et al.*, Phys. Rev. Lett. **107**, 045001 (2011).
[33] J. S. Liu, C. Q. Xia, W. T. Wang *et al.*, Phys. Rev. Lett. **107**, 035001 (2011).
[34] K. Schmid, L. Veisz, F. Tavella *et al.*, Phys. Rev. Lett. **102**, 124801 (2009).
[35] S. Banerjee, N. D. Powers, V. Ramanathan *et al.*, Phys. Plasmas **19**, 056703 (2012).
[36] S. Lacombe, L. Sabatier, F. Wien, and Y. A. Gauduel, Cell Death Dis. **1**, e4 (2010).
[37] B. Girolami, B. Larsson, M. Preger, C. Schaerf, and J. Stepanek, Phys. Med. Biol. **41**, 1581 (1996).
[38] K. J. Weeks, Nucl. Instrum. Methods Phys. Res., Sect. A **393**, 544 (1997).
[39] D. Habs, T. Tajima, J. Schreiber, C. P. J. Barty, M. Fujiwara, and P. G. Thirolf, Eur. Phys. J. D **55**, 279 (2009).
[40] H. A. Weidenmüller, Phys. Rev. Lett. **106**, 122502 (2011).